PAPER

Check for updates

A Raman spectroscopic and *ab initio* investigation of aqueous boron speciation under alkaline hydrothermal conditions: evidence for the structure and thermodynamic stability of the diborate ion†

Swaroop Sasidharanpillai, [ID] [a] Jenny S. Cox, [ID] [a] Cory C. Pye [ID] [b] and Peter R. Tremaine [ID] *[a]

Raman spectra of aqueous sodium borate solutions, with and without excess NaOH, NaCl, and LiCl, have been obtained from perpendicular and parallel polarization measurements acquired using a custom-built sapphire flow cell over the temperature range 25 to 300 °C at 20 MPa. The solvent-corrected reduced isotropic spectra include a large well-defined band at 865 cm^{-1} which overlaps with the boric acid B(OH)$_3$ band at 879 cm^{-1}, and becomes increasingly intense at elevated temperatures. This band does not correspond to the spectrum of any other previously reported aqueous polyborate ions, all of which have symmetric stretching bands at frequencies below that of borate, [B(OH)$_4$]$^-$, at 745 cm^{-1}. Based on the classic high-temperature potentiometric titration study by R. E. Mesmer, C. F. Baes and F. H. Sweeton, Acidity measurements at elevated temperatures. VI. Boric acid equilibriums, *Inorg. Chem.*, 1972, 11, 537–543, the new band was postulated to arise from a diborate ion, [B$_2$(OH)$_7$]$^-$ or [B$_2$O(OH)$_5$]$^-$. *Ab initio* density functional theory (DFT), together with chemical modelling studies, suggest that it is most likely [B$_2$(OH)$_7$]$^-$. Thermodynamic formation quotients derived from the peak areas showed variations with ionic strength as well as charge-balance discrepancies, which suggest one or more unidentified minor equilibrium species may also be present. The most likely candidate is the divalent diborate species [B$_2$O$_2$(OH)$_4$]$^{2-}$ which is also predicted to have a band near 865 cm^{-1} and is postulated to be present as a sodium ion pair. These are the first quantitative Raman spectra ever reported for borate-rich solutions under such conditions and provide the first spectroscopic evidence of a diborate species at PWR reactor coolant temperatures.
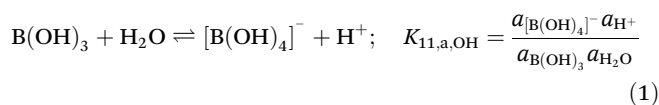
1. Introduction

An understanding of boric acid chemistry is essential to the nuclear industry, as boron containing compounds are added to the primary coolant in order to control the neutron flux in high-temperature pressurized water reactors (PWRs). Aqueous boric acid solutions can be highly complex; at least 10 different polyborate species are known to exist in solution depending on the specific conditions. Various spectroscopic techniques such as UV-visible spectroscopy,[1] infrared spectroscopy,[2] Raman spectroscopy,[3–10] X-ray diffraction,[5,11] dielec-

tric relaxation spectroscopy[12] and NMR[13] have previously been used to study aqueous boron species in order to identify different species and deduce their structures. The two principal challenges in studying boron species are the diversity of polyborate species that can co-exist at equilibrium under a wide range of conditions, and the experimental challenges associated with the quantification of these species under hydrothermal conditions.

The classical high-temperature potentiometric titration study of polyborate formation constants by Mesmer *et al.*[14] showed that, at temperatures up to 200 °C, the principal reactions are the ionization of boric acid,

*[a]Department of Chemistry, University of Guelph, Guelph, ON, Canada, N1G 2W1.
E-mail: tremaine@uoguelph.ca*
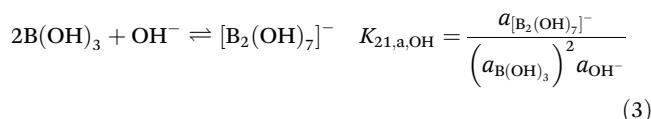*[b]Department of Chemistry, Saint Mary's University, Halifax, NS, Canada, B3H 3C3*
†Electronic supplementary information (ESI) available. See DOI: https://doi.org/10.1039/d3dt02514d

$$\text{B(OH)}_3 + \text{H}_2\text{O} \rightleftharpoons [\text{B(OH)}_4]^- + \text{H}^+; \quad K_{11,\text{a,OH}} = \frac{a_{[\text{B(OH)}_4]^-} a_{\text{H}^+}}{a_{\text{B(OH)}_3} a_{\text{H}_2\text{O}}}$$

(1)

and the formation of the triborate, tetraborate and/or pentaborate ions by ionization/condensation reactions such as:[15]

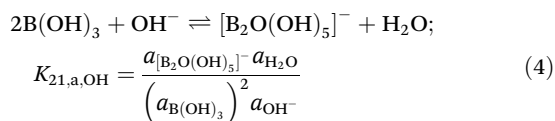$$xB(OH)_3 + yOH^- \rightleftharpoons [B_x(OH)_{3x+y}]^{y-} \tag{2}$$
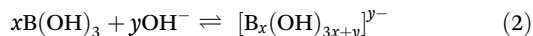
as well as more complicated stoichiometries. Subsequent studies by Raman spectroscopy and other methods noted above, confirmed the stoichiometries to be $[B_3O_3(OH)_4]^-$, $[B_4O_5(OH)_4]^{2-}$, and $[B_5O_6(OH)_4]^-$, respectively.[6,9]
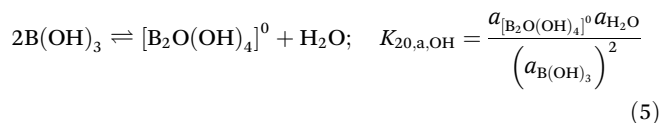
Although no spectra for diborate or metaborate species have been previously reported in aqueous solutions under ambient conditions, these species may be important under the high-temperature, high-pressure conditions encountered in nuclear reactor coolant. The potentiometric titration experiments reported by Mesmer and others[14–16] are able to determine the boron stoichiometry and charge, but not the degree of hydration or structure, of the aqueous species in their speciation models. The diborate species inferred from potentiometric measurements, which is postulated to be either $[B_2(OH)_7]^-$ or $[B_2O(OH)_5]^-$, forms through the reactions:
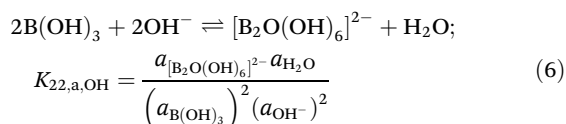
$$2B(OH)_3 + OH^- \rightleftharpoons [B_2(OH)_7]^- \quad K_{21,a,OH} = \frac{a_{[B_2(OH)_7]^-}}{\left(a_{B(OH)_3}\right)^2 a_{OH^-}} \tag{3}$$

or

$$2B(OH)_3 + OH^- \rightleftharpoons [B_2O(OH)_5]^- + H_2O;$$
$$K_{21,a,OH} = \frac{a_{[B_2O(OH)_5]^-} a_{H_2O}}{\left(a_{B(OH)_3}\right)^2 a_{OH^-}} \tag{4}$$

Although neutral and divalent diborates may form through condensation reactions, such as:

$$2B(OH)_3 \rightleftharpoons [B_2O(OH)_4]^0 + H_2O; \quad K_{20,a,OH} = \frac{a_{[B_2O(OH)_4]^0} a_{H_2O}}{\left(a_{B(OH)_3}\right)^2} \tag{5}$$

and

$$2B(OH)_3 + 2OH^- \rightleftharpoons [B_2O(OH)_6]^{2-} + H_2O;$$
$$K_{22,a,OH} = \frac{a_{[B_2O(OH)_6]^{2-}} a_{H_2O}}{\left(a_{B(OH)_3}\right)^2 (a_{OH^-})^2} \tag{6}$$

there is no evidence for them in the potentiometric studies reported to date.

The present study reports the reduced isotropic Raman spectra for sodium borate solutions under alkaline conditions at temperatures up to 300 °C at 20 MPa, using a newly designed titanium-alloy flow cell with sapphire windows.[8] The characteristic vibrational frequencies and relative scattering coefficients reported by Applegarth *et al.*[9] were used to calculate the equilibrium concentrations of the polyborate species from the reduced isotropic Raman spectra. The assignment of bands to the diborate species, and the relative intensities of the major peaks in the spectrum of each species, was based on density functional theory (DFT) calculations using Gaussian 03 software at several levels of theory with, and without, the polar-

izable continuum model solvation shell. These experimental results are not consistent with speciation calculations from the two different chemical equilibrium models of interest to the nuclear industry under these conditions, the OLI Analyzer Studio 9.2.1 software[17] and the EPRI MULTEQ software (ChemWorks 4.0, MULTEQ database v. 7.0).[18,19] The speciation results from the Raman measurements were used to calculate new values for the thermodynamic formation quotients of the diborate ion. These are the first quantitative Raman spectra ever reported for borate-rich solutions under hydrothermal conditions and provide the first spectroscopic evidence of a diborate species at PWR reactor coolant temperatures.

2. Experimental

2.1. Chemical and solution preparation

Boric acid, $B(OH)_3$, (Alfa Aesar, 99.9995%), NaCl (Sigma, 99.5%), LiCl (Sigma-Aldrich, 99+%), and potassium hydrogen phthalate (KHP) (Fisher Scientific, 99.95%), were dried in an oven to constant mass before use. Sodium perchlorate (Alfa Aesar, ACS anhydrous grade, 98–102%) was used without further treatment. Carbonate-free stock solutions of 0.998 mol kg^{-1} and 1.023 mol kg^{-1} NaOH were prepared by mass from 50% w/w aqueous solution (Alfa Aesar) and standardized by triplicate titrations against KHP.

All borate solutions were prepared by adding a calculated mass of $B(OH)_3$ to a 0.998 mol kg^{-1} or 1.023 mol kg^{-1} NaOH solution to obtain the desired $B(OH)_3$ molality in the final solution. Sodium perchlorate (0.1 mol kg^{-1}) was added to all solutions as an internal reference standard. All solutions were prepared by mass to an estimated standard uncertainty of ±0.5%, using 18.2 MΩ cm ultrapure water from a Millipore Direct-Q 5 water purification system, and stored in sealed Nalgene bottles until used. For the solutions requiring higher NaOH molalities (buffer ratios >1), additional 50% w/w NaOH, whose composition had been quantified during the preparation of the 0.998 mol kg^{-1} and 1.023 mol kg^{-1} NaOH solutions, was added by mass. These were estimated to have a larger standard uncertainty, ±2%.

The stoichiometric buffer ratios of these solutions,

$$R_{Buffer} = m_{NaOH}^{ST}/m_{B(OH)_3}^{ST} = \left(m_{Na_{Total}} - m_{ClO_4^-}\right)/m_{B_{Total}} \tag{7}$$

refer to the stoichiometric molality ratio of NaOH to $B(OH)_3$ used to make the solutions, m_{NaOH}^{ST} and $m_{B(OH)_3}^{ST}$. Thus, ($R_{Buffer} = 0$, $m_B = 0.80$ mol kg^{-1}) refers to a pure $B(OH)_3$ solution with $m_{B(OH)_3}^{ST} = 0.80$ mol kg^{-1} and $m_{NaOH}^{ST} = 0.00$ mol kg^{-1}, and ($R_{Buffer} = 1.0$, $m_B = 1.0$ mol kg^{-1}) refers to an aqueous solution of sodium borate with $m_{B(OH)_3}^{ST} = 1.00$ mol kg^{-1} and $m_{NaOH}^{ST} = 1.00$ mol kg^{-1}.

In order to determine the effects of ion-pair formation and ionic strength, solutions of $NaB(OH)_4$ ($R_{Buffer} = 0.980$, $m_B = 0.320$ mol kg^{-1}) and $LiB(OH)_4$ ($R_{Buffer} = 1.000$, $m_B = $ and 0.310 mol kg^{-1}) were prepared using the procedures described above, to which an approximately equimolal excess of NaCl or LiCl was added by mass.

2.2. Raman spectroscopy and titanium sapphire flow cell

The reduced isotropic spectra of the borate solutions described above were measured from 25 to 300 °C at 20 MPa using a novel custom-made sapphire flow cell described previously in detail by Sasidharanpillai et al.[8] The whole assembly was fitted into a Teflon cell holder in a fixed position on the translation stage of the Raman microscope. Experiments were carried out in constant flow mode at a flow rate of 0.5 ml min^{-1}, with temperature controlled to within ±1 °C over the several hours required to make each set of measurements. Constant pressure in the line was maintained using a syringe pump (Teledyne ISCO Inc.) filled with ultrapure water and a backpressure regulator (TESCOM 26-1722-24) located at the end of the flow line. The solutions to be studied were pumped through the cell using a 24 mL sample injection loop on a Rheodyne injector.

Raman spectra were obtained from polarized back-scattering measurements at constant temperature using a custom-made Horiba Jobin Yvon HR800 LabRAM system constructed with a fiber-optic coupled OLYMPUS confocal microprobe, using a 532 nm laser exciting line and a super-long-working-distance achromatic 20× objective lens (SLMPlan, OLYMPUS). Spectra were collected with polarizers set parallel and perpendicular to the polarization of exciting beam such that a baseline-corrected reduced isotropic spectra could be obtained, following the experimental protocol from Sasidharanpillai et al.[8]

The solvent-subtracted baseline-corrected spectra for quantitative equilibrium constants were obtained by recording the spectra of the water blanks and solutions, using both polarizations as a series on the same day, with the flow cell in a fixed position under the confocal microscope at constant temperature and pressure. Each Raman spectrum for the parallel (||) and perpendicular (⊥) polarizations was the average of eight runs in order to reduce the background noise. A perchlorate standard solution was injected at the beginning and end of the day's runs, and these spectra varied by <5% during the course of the day, indicating the laser power remained constant during the full set of runs. The temperature thermostatting over the course of each day was constant to ±2 °C or better.

Isotropic Raman spectra, $I_{Iso}(\tilde{\nu})$, were obtained from the parallel (||) and perpendicular (⊥) polarized spectra using previously described methods.[8,9,20] The isotropic water spectrum was subtracted to obtain each solvent-corrected isotropic spectrum $I_{Iso}(\tilde{\nu})$.[8,9,20] The reduced isotropic spectra, $R_{Iso}(\tilde{\nu})$ was obtained by correcting for the frequency dependence and the Boltzmann distribution.[8,20] An example of the experimental Raman spectra for both solution and water at parallel and perpendicular polarizations, the isotropic spectra of the solution and solvent, and the resulting solvent-corrected isotropic spectrum is shown in ESI (Fig. S1†).

2.3. Ab initio and DFT calculations

Calculations were performed using Gaussian 03 software, with MP2 calculations carried out using the frozen core approximation. The geometries were optimized using a stepping stone approach, in which the geometries at the levels HF/6-31G*, HF/6-31+G*, HF/6-311+G*, B3LYP/6-31G*, B3LYP/6-31+G*, B3LYP/6-311+G*, MP2/6-31G*, MP2/6-31+G*, and MP2/6-311+G* were sequentially optimized, and the geometry and molecular orbital reused as an initial guess for the subsequent level. Default optimization specifications were generally used. After each optimization, a frequency calculation was performed at the same level and the resulting Hessian was used in the subsequent optimization. Symmetry-constrained Z-matrix coordinates were used to speed up the optimizations. If imaginary frequencies were found, then the symmetry was lowered along the appropriate irreducible representation and the process was repeated. The Hessian was evaluated at the first geometry (Opt = CalcFC) for the first level in a series in order to aid geometry convergence. Full details of the computational methods are reported elsewhere.[21] The Raman intensities and depolarization ratios were calculated by default for Hartree–Fock calculations; for B3LYP and MP2 calculations, these were done by specifying Freq = Raman. For selected structures, the process was repeated with the conductor-like polarizable-continuum solvation model (SCRF = CPCM). Calculations for the divalent diborate species and the triborate species were done with Gaussian 16.

3. Raman spectroscopic results

3.1. Reduced isotropic Raman spectra

Fig. 1 displays a plot of the reduced isotropic Raman spectra of an aqueous solution prepared with equal ratios of NaOH and boric acid (Solution 1, R_{Buffer} = 0.980, m_B = 1.019 mol kg^{-1}) for temperatures from 25 °C to 300 °C at 20 MPa. At 25 °C, there are two peaks at 745 cm^{-1} and 936 cm^{-1}, which correspond to
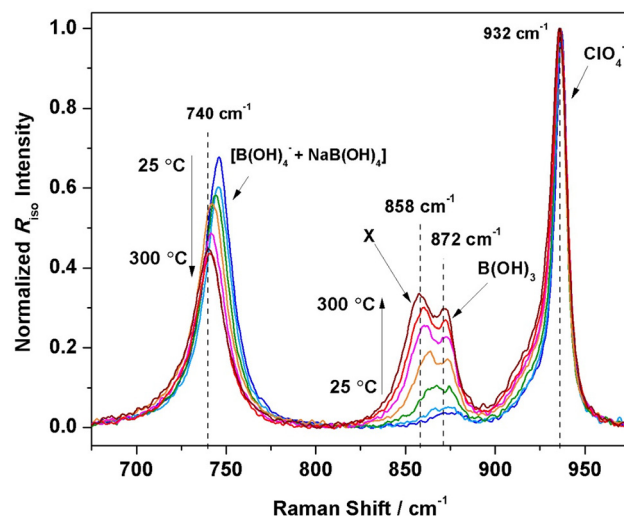

Fig. 1 Reduced isotropic Raman spectra, $R_{Iso}(\tilde{\nu})$, of NaB(OH)$_4$ (aq.) at temperatures from 25 to 300 °C and 20 MPa for Solution 1, Run 1 (R_{Buffer} = 0.980, m_B = 1.019 mol kg^{-1}, with 0.0902 mol kg^{-1} sodium perchlorate). The spectra are normalized with respect to the perchlorate internal standard peak. The frequencies shown are peak positions at 300 °C.

$[B(OH)_4]^-$ and the $[ClO_4]^-$ internal standard, respectively. At temperatures above 75 °C, two overlapping peaks appear, with maxima at ~865 and ~875 cm^{-1}, whose intensities increase as the temperature is increased. The band at ~875 cm^{-1} is clearly the $B(OH)_3$ symmetric stretch, however, the lower frequency shoulder at ~865 cm^{-1} does not correspond to any previously reported aqueous borate or polyborate species. The $B(OH)_3$ peak and the unknown peak (marked as "Species X") were not well resolved at lower temperatures, but became better resolved above 150 °C. At higher temperatures, the borate peak intensity decreased, while the intensities of the $B(OH)_3$ band and the unknown peak both increased. All peaks shifted to lower energies with increasing temperature.

To confirm that the new species is an equilibrium species at high temperature, reduced isotropic Raman spectra for a solution of (R_{Buffer} = 0.980, m_B = 1.019 mol kg^{-1}, with 0.0902 mol kg^{-1} sodium perchlorate) were recorded at 22 °C, then again after heating to 200 °C, and a final time after cooling it back to 22 °C (ESI, Fig. S2†). Both spectra at 22 °C were identical and showed the presence of only the borate and perchlorate peaks, while the spectrum at 200 °C clearly indicated three peaks (borate, unknown species X, and boric acid). This showed that the new species at 865 cm^{-1} was formed only at high temperatures, and that the reaction is reversible.

The Raman spectra for Solution 1 (R_{Buffer} = 0.980, m_B = 1.019 mol kg^{-1}, and perchlorate standard) were run in dupli-

Table 1 Relative peak areas[a] for the boron and polyborate species with respect to the perchlorate internal standard, calculated from the reduced isotropic Raman spectra of NaB(OH)$_4$ at 20 MPa, with and without excess NaOH from 25 to 300 °C

	745 cm^{-1} band		865 cm^{-1} band		875 cm^{-1} band	
	$[NaB(OH)_4]^0$ + $[B(OH)_4]^-$ + "Unknown(s)"		"Unknown X"		$B(OH)_3$	
t/°C	ν/cm^{-1}	Area	ν/cm^{-1}	Area	ν/cm^{-1}	Area
	Solution 1 (Run 1), R_{Buffer} = 0.980, m_B = 1.0188 mol kg^{-1}, m_{NaClO_4} = 0.0902 mol kg^{-1}					
150	745	1.126 ± 0.066	866	0.128 ± 0.009	875	0.046 ± 0.003
200	742	1.084 ± 0.082	863	0.225 ± 0.018	873	0.108 ± 0.009
250	741	0.895 ± 0.034	862	0.361 ± 0.015	872	0.170 ± 0.010
275	740	0.787 ± 0.041	861	0.450 ± 0.024	872	0.181 ± 0.010
300	740	0.894 ± 0.028	858	0.469 ± 0.016	872	0.211 ± 0.007
	Solution 1 (Run 2), R_{Buffer} = 0.980, m_B = 1.0188 mol kg^{-1}, m_{NaClO_4} = 0.0902 mol kg^{-1}					
150	742	1.147 ± 0.073	866	0.146 ± 0.010	874	0.054 ± 0.005
200	741	1.038 ± 0.075	863	0.252 ± 0.020	873	0.082 ± 0.008
250	740	0.894 ± 0.090	859	0.382 ± 0.039	872	0.158 ± 0.016
	Solution 2, R_{Buffer} = 0.984, m_B = 1.0391 mol kg^{-1}, m_{NaClO_4} = 0.0955 mol kg^{-1}					
150	741	1.112 ± 0.037	866	0.132 ± 0.009	873	0.043 ± 0.008
200	740	0.958 ± 0.046	862	0.227 ± 0.013	872	0.099 ± 0.006
250	739	0.809 ± 0.053	859	0.342 ± 0.024	870	0.155 ± 0.011
	Solution 3, R_{Buffer} = 1.716, m_B = 0.96404 mol kg^{-1}, m_{NaClO_4} = 0.0945 mol kg^{-1}					
150	744	1.161 ± 0.033	864	0.192 ± 0.007	NA	NA
200	743	1.044 ± 0.081	863	0.260 ± 0.021	NA	NA
250	741	0.930 ± 0.057	858	0.405 ± 0.026	NA	NA
	Solution 4, R_{Buffer} = 3.542, m_B = 0.90062 mol kg^{-1}, m_{NaClO_4} = 0.0883 mol kg^{-1}					
150	744	1.237 ± 0.043	865	0.132 ± 0.010	NA	NA
200	743	0.983 ± 0.041	864	0.246 ± 0.012	NA	NA
250	741	0.901 ± 0.040	859	0.302 ± 0.017	NA	NA
	Solution 5a, R_{Buffer} = 0.980, m_B = 0.32012 mol kg^{-1}, m_{NaClO_4} = 0.0283 mol kg^{-1}					
250	740	0.818 ± 0.043	859	0.434 ± 0.026	872	0.286 ± 0.016
	Solution 5b, R_{Buffer} = 0.980, m_B = 0.32012 mol kg^{-1} + 0.301 mol kg^{-1} NaCl, m_{NaClO_4} = 0.0283 mol kg^{-1}					
250	740	0.864 ± 0.061	859	0.462 ± 0.036	872	0.252 ± 0.019
	Solution 6a[b], R_{Buffer} = 1.000, m_B = 0.30980 mol kg^{-1}, m_{NaClO_4} = 0.0330 mol kg^{-1}					
250	740	0.535 ± 0.029	859	0.297 ± 0.019	872	0.229 ± 0.013
	Solution 6b[b], R_{Buffer} = 0.980, m_B = 0.30980 mol kg^{-1} + 0.302 mol kg^{-1} LiCl, m_{NaClO_4} = 0.0330 mol kg^{-1}					
250	740	0.658 ± 0.041	740	0.384 ± 0.029	740	0.269 ± 0.019

[a] Standard uncertainties, ±, were taken to be equal to the relative standard errors of the Voight function fits to the perchlorate and species bands.
[b] LiB(OH)$_4$ solution.

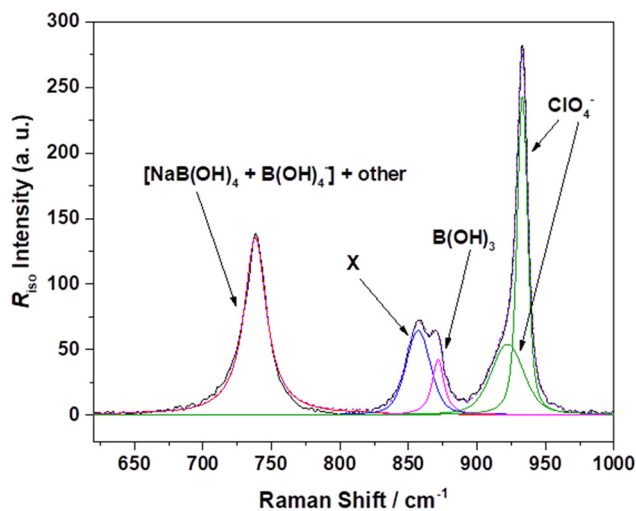**Fig. 2** Reduced isotropic Raman spectra of NaB(OH)$_4$ (aq.), $R_{Iso}(\bar{\nu})$, at 250 °C and 20 MPa, showing the fitted Voight functions used to determine peak positions and peak areas relative to the perchlorate internal standard for Solution 1, Run 1 (R_{Buffer} = 0.980, m_B = 1.019 mol kg^{-1}, 0.0902 mol kg^{-1} sodium perchlorate). Where "X" is diborate, Fig. 6 is believed to be a more accurate representation of the individual species bands.

cate on a separate day, at 20 MPa and temperatures from 25 to 250 °C, and a second solution with similar composition (Solution 2, Table 1) was also run under the same conditions. Peak fitting to integrate the area under each band was done with a Voigt function using the curve fitting function in Origin Pro 2016 software. The fitting parameters for the position and the Lorentzian and Gaussian widths of the boric acid peak at each temperature were constrained to be same as those reported by Sasidharanpillai *et al.*,[8] for the boric acid peak in a 0.780 molal boric acid solution acquired with the same instrument under similar experimental conditions. As an example, the deconvoluted spectrum of Solution 1 at 250 °C is shown in Fig. 2. The areas were determined as the areas of peaks for species *i* relative to the perchlorate internal standard, A_i/A_{IS}. Following established practice,[8] the sum of the areas of the two peaks at ~935 cm^{-1} and ~920 cm^{-1} was used in the calculation of the total area of the perchlorate band. The standard errors in the relative areas for the boron bands were 10% or less. The solutions and initial concentrations run in this study, together with the frequencies and relative peak areas corresponding to each of the deconvoluted Raman bands, are tabulated in Table 1.

We measured Raman spectra at 250 °C using sodium borate solutions in D$_2$O with isotopically pure B(OD)$_3$ and NaOD, similar in composition to Solutions 1, 3 and 4, in an attempt to confirm the identification of diborate species. This single set of runs using isotopically pure B(OD)$_3$ and NaOD consumed about 1000 mL D$_2$O. Complications arising from the Fermi resonance effects in the spectra for B(OD)$_3$ and the shifts in speciation associated with the deuterium isotope effect on its ionization constant proved too difficult to resolve.[22,23] Details are reported in ESI section S2.†

3.2. The effect of excess Na$^+$ and Li$^+$ cations and possible ion pairing

Previous Raman experiments on boric acid/borate confirmed that Raman spectroscopy cannot distinguish between free borate [B(OH)$_4$]$^-$ and the ion pair [NaB(OH)$_4$]^0, possibly because [NaB(OH)$_4$]^0 exists as solvent-separated ion pairs.[9] Reduced isotropic Raman spectra for NaB(OH)$_4$ and LiB(OH)$_4$ solutions (Solution 5: R_{Buffer} = 0.980, m_B = 0.320; and Solution 6: R_{Buffer} = 0.980, m_B = 0.310 mol kg^{-1}; respectively), and the spectra of the same solutions to which an approximately equimolal excess of NaCl or LiCl had been added, were recorded at 250 °C and 20 MPa. Fig. 3 shows the isotropic spectra and corresponding deconvolution of peaks for Solution 5a (R_{Buffer} = 0.980, m_B = 0.320) and Solution 5b (R_{Buffer} = 0.980, m_B = 0.320, m_{NaCl} = 0.301) at 250 °C and 20 MPa. The similarity in the spectra and corresponding deconvolution for solutions with
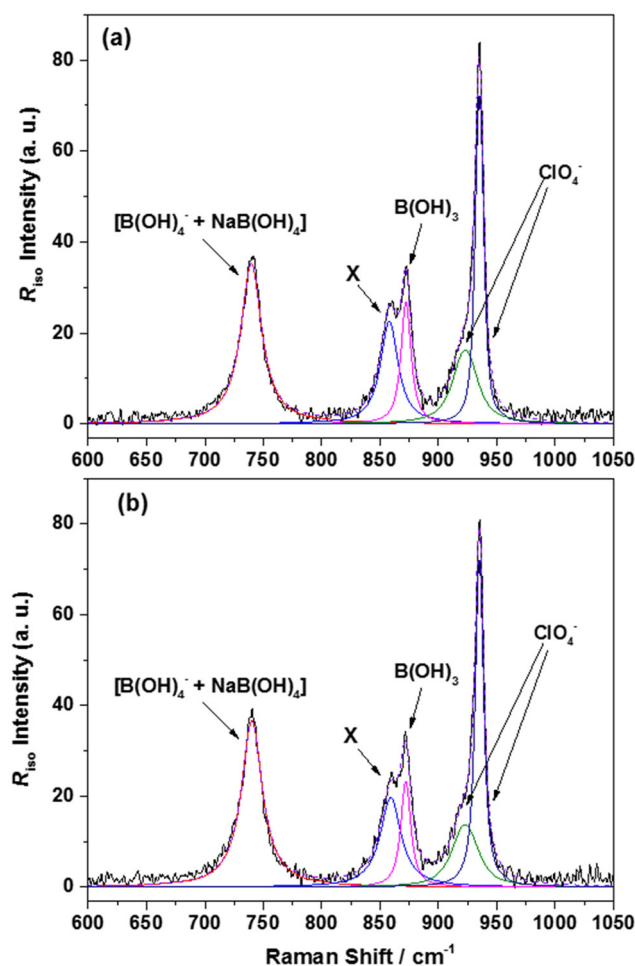

Fig. 3 Reduced isotropic Raman spectra of NaB(OH)$_4$(aq.) with and without NaCl(aq.), $R_{Iso}(\bar{\nu})$, at 250 °C and 20 MPa, showing the fitted Voight functions used to determine peak positions and peak areas relative to the perchlorate internal standard. (a) Solution 5a: R_{Buffer} 0.980, m_B = 0.32012 mol kg^{-1} with 0.0283 mol kg^{-1} sodium perchlorate and (b) Solution 5b: R_{Buffer} = 0.980, m_B = 0.32012 mol kg^{-1} + 0.301 mol kg^{-1} NaCl with 0.0283 mol kg^{-1} sodium perchlorate.

and without excess NaCl/LiCl indicates that the presence and identity of the cation does not affect the concentration of the unknown species, and confirms either that the new band does not result from ion-pair formation, or that there is extensive ion pairing in even the dilute $NaB(OH)_4$ and $LiB(OH)_4$ solutions. The frequencies and relative peak areas are reported in Table 1.

3.3. The effect of excess hydroxide

The Raman spectra of solutions of different R_{Buffer} values ≥ 1 were recorded at 150, 200 and 250 °C and 20 MPa in order to understand the effect of hydroxide ion on the equilibrium reactions responsible for the newly observed species. The reduced isotropic Raman spectra and peak deconvolution of Solutions 3 (R_{Buffer} = 1.716) and 4 (R_{Buffer} = 3.542) at 250 °C and 20 MPa, are shown in Fig. 4. When the concentration of

hydroxide ion was increased, the boric acid peak became negligible, and only the bands associated with the borate ion and the new species could be observed. The frequencies and peak areas of each band are listed in Table 1. The ratio of the peak areas for the bands at 865 cm^{-1} and 745 cm^{-1}, A_{865}/A_{745}, increased with temperature, and did not depend strongly on the hydroxide concentration.

4. *Ab initio* and DFT computational results

4.1. Borates, diborates, and higher polyborates

In a previous study on polyborates by Applegarth *et al.*[9] at 25 and 80 °C, the predicted isotropic Raman spectra of boric acid, $B(OH)_3$; borate ion, $[B(OH)_4]^-$; the oxo-bridged diborates $[B_2O(OH)_6]^{2-}$ and $[B_2O(OH)_5]^-$; the cyclic triborate ion, $[B_3O_3(OH)_4]^-$; metaboric acid, $B_3O_3(OH)_3$; tetraborate, $[B_4O_5(OH)_4]^{2-}$; and the pentaborates $[B_5O_6(OH)_4]^-$ and $[B_5O_6(OH)_6]^{3-}$, were discussed and compared with experimental results. The frequencies for boric acid, borate, and the higher polyborates were reported by Applegarth *et al.*[9] It was shown that the frequencies of unscaled MP2 and B3LYP low-temperature Raman spectra compared very favorably with experimental results for $B(OH)_3$, $[B(OH)_4]^-$, $[B_3O_3(OH)_4]^-$, $[B_4O_5(OH)_4]^{2-}$, and $[B_5O_6(OH)_4]^-$, suggesting that these were the observed species. There was no experimental evidence from the Raman spectra for the presence of either $[B_2O(OH)_6]^{2-}$ or $[B_2O(OH)_5]^-$ at these temperatures, consistent with the recently completed detailed NEA/OECD literature review by the Thermodynamic Database Project.[24] Generally speaking, the MP2 and B3LYP results were found to underestimate the experimental frequencies by up to 35 cm^{-1} because the effect of the solvent was not explicitly included in these calculations, and this effect increased with the overall charge of the species. Hartree Fock calculations, which were also carried out, were found to overestimate the frequencies by a larger, less predictable amount.

The high-temperature Raman results obtained in this study were used to direct our calculations. These suggest that there is an additional species in equilibrium with $B(OH)_3$ and $[B(OH)_4]^-$, which gives rise to a characteristic Raman band at 865 cm^{-1}, concomitant with dissociation of borate into boric acid. Based on the known spectra of the boric acid/borate solutions at 25 °C,[9] the most likely candidates are the metaborate ion, $[BO(OH)_2]^-$; one of four diborate species, $[B_2O(OH)_5]^-$, $[B_2O_3(OH)_4]^{2-}$, $[B_2O(OH)_6]^{2-}$ or $[B_2(OH)_7]^-$; or a higher polyborate species (possibly $[B_3O_3(OH)_5]^{2-}$) that is not a significant species at 25 °C. Less likely neutral species that might result from the condensation reactions of boric acid, driven by higher ionic strength or temperature, are $[B_2(OH)_6]^0$ and $[B_2O(OH)_4]^0$.

Ab initio computational studies on these species were carried out at several levels of theory, with and without solvation, as discussed in the following section. Selected gas-phase structures were taken from previous studies of Pye *et al.*[21,25] The structures of the diborate species derived from
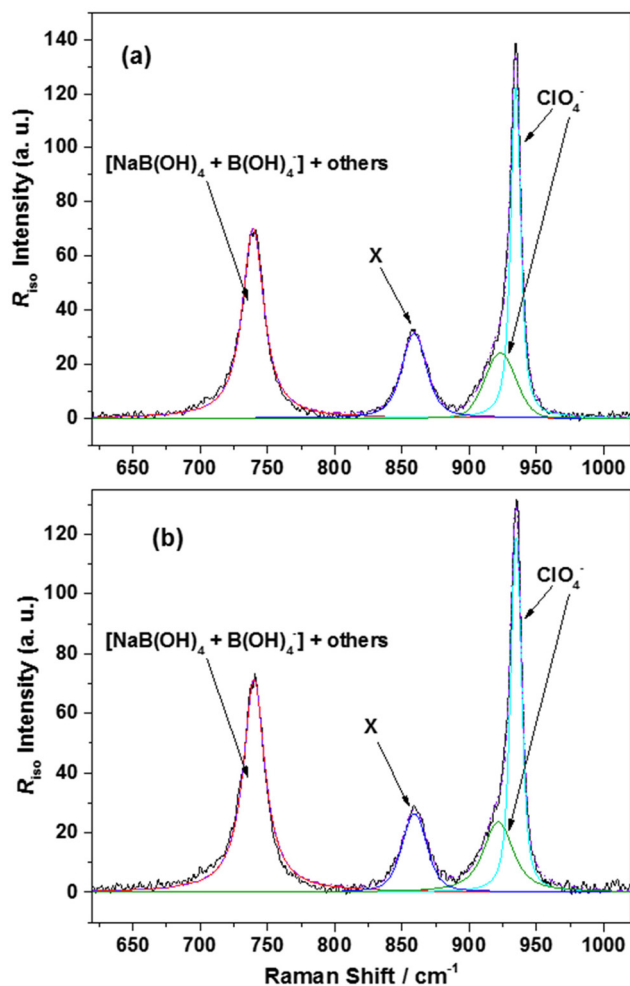

Fig. 4 Reduced isotropic Raman spectra of $NaB(OH)_4$(aq.) with excess NaOH(aq.), $R_{Iso}(\tilde{\nu})$, at 250 °C and 20 MPa, showing the fitted Voight functions used to determine peak positions and peak areas relative to the perchlorate internal standard. (a) Solution 3: R_{Buffer} = 1.716, m_B = 0.96404 mol kg^{-1}, with m_{NaClO_4} = 0.0945 mol kg^{-1} sodium perchlorate; (b) Solution 4: R_{Buffer} = 3.542, m_B = 0.90062 mol kg^{-1}, with 0.0883 mol kg^{-1} sodium perchlorate.
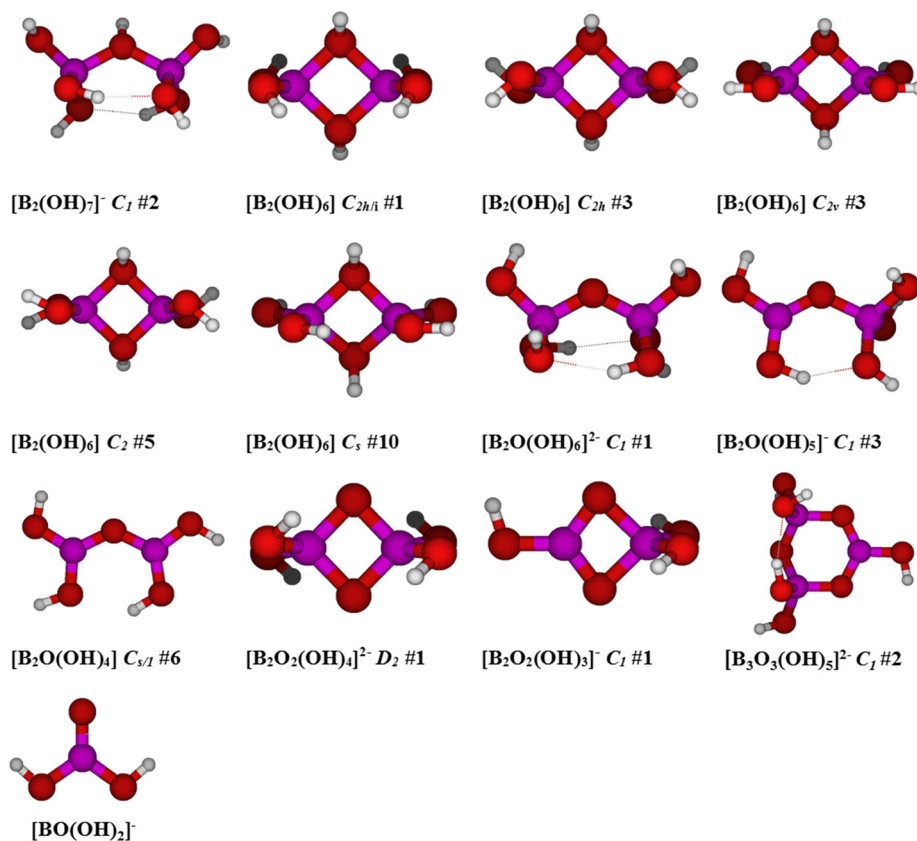
Fig. 5 Calculated structures (using Gaussian 03) of the postulated diborate species considered for the unknown Raman peak at 865 cm^{-1}, along with their symmetry.

these calculations in this study are shown in Fig. 5. Gas-phase Raman frequency calculations were done for a broader number of potential di/triborate species initially, with results listed in ESI (Table S1†). The Raman frequencies and the corresponding isotropic Raman activities for the ionic di/triborate species in solution phase are tabulated in Table 2.

4.2. Neutral diborate species

4.2.1. Boric acid dimer, $[B_2(OH)_6]^0$. The possibility of a neutral dimer of boric acid, $[B_2(OH)_6]^0$, was explored computationally. Initial attempts to locate a C_s-symmetric dimer with a single bridging hydroxyl group resulted in dissociation to a hydrogen-bonded boric acid dimer $[B(OH)_3]_2$, thus systematic desymmetrization from a high symmetry structure was attempted. Neither of the two D_{2h} forms are minima, but, unexpectedly, some of the C_{2v} and C_{2h} structures were. Some C_{2h} structures broke two B–O bonds during optimization to give two molecules of boric acid. Furthermore, some additional minima were found, of C_2 and C_s symmetry. Of all of the potential structures, C_{2v} #3 was the most stable, however, the calculated isotropic Raman modes corresponding to B–O stretching and/or deformation are too low in frequency. The gas-phase dimerization energy was also calculated to be prohibitively large for any appreciable amount to coexist with boric acid (35–104 kJ mol^{-1}).

4.2.2. Oxo-bridged dimer of boric acid, $[B_2O(OH)_4]^0$. The dehydrated oxo-bridged dimer of boric acid, $[B_2O(OH)_4]^0$, was also considered. None of the four possible C_{2v} structures were stable, but the corresponding C_2 structures were, in which the BO$_3$ subunits have twisted out of the plane of the B–O–B bridge. These C_s structures formed by rotating hydroxyl groups and containing an internal hydrogen bond, were also stable, with C_s #6 being the most stable overall; however, the most intense band in the isotropic Raman spectrum was predicted to be too low (770–780 cm^{-1}) to make this a reasonable possibility.

4.3. Ionic diborate species

4.3.1. The diborate ion, $[B_2(OH)_7]^-$. The diborate ion identified in the potentiometric study by Mesmer *et al.*[14] was postulated to be $[B_2(OH)_7]^-$. The computational methods employed here indicate that neither of the two C_{2v} forms are minima on the potential energy surface, and the same is true of the two C_2 and four C_s structures derived from them. In fact, one of the C_s structures dissociates into boric acid and borate. However, two minimum-energy C_1 structures do exist, of which the second is slightly more stable. This species is predicted to have two intense bands in the isotropic Raman spectrum below 1000 cm^{-1}, where the higher but less intense band for B3LYP calculations gives a reasonable match to experiment.

Table 2 *Ab initio* calculated vibrational frequencies (cm^{-1}) and Raman activities of perchlorate, postulated diborate species, and metaborate ion in the solution phase (Polarized Continuum Model)

Species	Basis set	HF		B3LYP		MP2	
		ν/cm^{-1}	Raman activity	ν/cm^{-1}	Raman activity	ν/cm^{-1}	Raman activity
ClO_4^-	6-31G*	987	37.8	864	56.4	994	50.2
	6-31+G*	970	62.5	831	116	973	106
	6-311+G*	959	58.8	816	112	950	98.4
$[B_2O(OH)_5]^-$	6-31G*	759	4.77	713	7.82	731	8.29
		983	1.82	925	4.41	932	4.12
	6-31+G*	748	5.09	572	1.11	581	1.18
		771	2.74	707	11.2	722	13.9
		975	3.35	913	8.76	922	8.55
	6-311+G*	749	5.35	574	1.09	587	1.23
		773	1.57	703	9.78	728	13.1
		853	0.57	792	1.05	813	0.23
		972	3.02	911	8.75	925	8.44
$[B_2O(OH)_6]^{2-}$	6-31G*	749	7.24	703	10.6	692	1.06
						719	10.2
	6-31+G*	743	11.1	692	2.44	700	2.14
				698	13.3	714	17.6
	6-311+G*	626	1.30	695	6.03	711	3.09
		742	10.5	696	11.1	725	17.5
$[B_2(OH)_7]^-$	6-31G*	730	4.85	616	1.64	631	2.03
		897	2.59	679	5.36	682	3.42
				752	2.99	696	2.06
				836	5.09	742	4.01
						857	3.84
	6-31+G*	623	1.13	566	1.01	590	2.58
		727	5.67	619	1.53	621	1.30
		890	6.16	689	8.29	691	5.66
				829	8.62	845	9.88
	6-311+G*	729	5.10	626	1.56	681	1.91
		885	5.97	690	7.55	719	8.66
				824	8.38	848	9.11
$[BO(OH)_2]^-$	6-31G*	884	5.46	826	8.10	837	9.71
		1144	3.11	1061	5.33	1067	5.97
				1555	1.60	1568	1.60
	6-31+G*	886	7.38	827	11.9	835	15.5
		1117	3.31	1031	4.86	1030	6.18
		1554	4.61	1457	17.3	1446	16.6
	6-311+G*	881	6.49	824	10.7	835	14.0
		1136	3.39	1048	4.76	1049	6.31
		1544	4.23	1449	17.3	1451	18.1
$[B_2O_2(OH)_4]^{2-}$	6-31G*	634	2.47	588	3.19	591	3.37
		922	8.58	845	10.93	846	13.06
	6-31+G*	636	4.72	593	6.35	591	7.35
		915	6.59	839	8.43	830	13.74
	6-311+G*	635	4.49	591	6.15	599	7.58
		910	6.49	834	8.30	836	12.55
$[B_3O_3(OH)_5]^{2-}$	6-31G*	581	2.66	551	2.75	553	2.76
		655	3.54	601	6.21	606	6.77
		792	3.59	731	5.91	733	7.58
	6-31+G*	576	2.86	533	3.79	536	4.50
		651	6.70	553	1.38	590	8.19
		790	4.01	587	5.20	622	5.45
				615	6.28	727	8.26
				727	4.96		
	6-311+G*	575	3.00	532	3.31	540	4.29
		651	5.99	551	2.60	562	1.66
		789	3.42	584	4.53	594	8.15
				612	5.78	632	3.77
				725	3.98	734	7.38

4.3.2. Oxo-bridged diborate ions $[B_2O(OH)_6]^{2-}$, $[B_2O(OH)_5]^-$, $[B_2O_2(OH)_4]^{2-}$, and $[B_2O_2(OH)_3]^-$. Frequency and isotropic Raman activity calculations for oxo-bridged diborate species were performed with same basis set as in the gas phase calculations, using a polarizable continuum model to simulate hydration effects.

The oxo-bridged diborates $[B_2O(OH)_6]^{2-}$ and $[B_2O(OH)_5]^-$ were previously considered[9] as candidates for the band at 773 cm^{-1}, observed as a shoulder on the borate peak at 745 cm^{-1}. $[B_2O(OH)_6]^{2-}$ may exist as an oxo-bridged dimer with one of two C_2 and three C_1 structures lying within 15 kJ mol^{-1} of each other, having weak bands at 812–870 cm^{-1} which appear in the correct region for matching with the experimental band at 865 cm^{-1}. $[B_2O(OH)_5]^-$ may exist as an oxo/hydroxo doubly bridged dimer, but these forms were not stable and resulted in cleavage of one of the B–μOH bonds upon relaxation of symmetry constraints, giving rise to one of nine possible oxo-bridged C_1 structures. $[B_2O(OH)_5]^-$ is calculated to have weak bands at 890–940 cm^{-1} which would be too high in frequency. Additionally, both of these species have an intense band predicted at lower frequencies (680–720 cm^{-1}), which is not experimentally observed.

Species containing two oxo bridges were also considered. $[B_2O_2(OH)_4]^{2-}$ may exist as one of two possible D_{2h} structures, neither of which was found to be stable. Desymmetrization can give rise to two D_2, four C_{2h}, and one C_{2v} structures. The D_2 #1 structure is the most stable at all levels, and the C_{2h} #1 and D_2 #2 structures are stable at some levels. For unstable structures, further desymmetrization give stable structures with C_2, C_i, and C_s symmetry. The two most intense bands of roughly equal intensity in the isotropic Raman spectrum are predicted at 570–580 cm^{-1} and 830–850 cm^{-1}, and these are expected to be systematically too low by about 20 cm^{-1}. The latter band, therefore, is a viable candidate for the experimentally observed band at 865 cm^{-1}, however, no evidence for the predicted weak band at around 600 cm^{-1} was observed in the experimental spectrum ($R_{Buffer} = 0.980$, $m_B = 1.019$ mol kg^{-1}). It is possible that these peaks would be obscured if $[B_3O_3(OH)_4]^-$ was present, but this does not appear to be the case for solutions of this composition.

The second possible species with two oxo bridges is $[B_2O_2(OH)_3]^-$, which could exist as one of two C_{2v} structures, neither of which is a minimum. Desymmetrization to one of two possible C_2 or four possible C_s structures also did not result in minima. Two C_1 structures exist, the first of which is the most stable, however, the calculations predict the existence of several intense bands in the 500–1000 cm^{-1} range and none of these are a satisfactory match to experiment. In addition, of the two bands that bracket the experimental value, it is the remaining two which would have the greatest intensity.

4.4. Ionic triborate species

4.4.1. The triborate ion, $[B_3O_3(OH)_5]^{2-}$. The cyclic divalent triborate ion was also examined. Neither of the two C_s forms were stable, and converted to the corresponding C_1 forms. Several intense isotropic bands in the range 500–800 cm^{-1} were noted. Most of the lower frequency bands correspond to HOB bending. It is unlikely that these would be observed in practice because the coupling with water librations in the first solvation shell would broaden the bands. No band at around 865 cm^{-1} was observed; however, a band predicted at ~730 cm^{-1}, which would be obscured under the experimentally observed borate peak at 745 cm^{-1}, may be a contributing factor to the apparent charge-balance discrepancy, noted below.

4.5. Solvent effects: CPCM calculations

Candidates for the unknown species were therefore reduced to $[B_2(OH)_7]^-$, $[B_2O(OH)_5]^-$, $[B_2O_2(OH)_4]^{2-}$, $[B_2O(OH)_6]^{2-}$ and $[BO(OH)_2]^-$ based on the frequencies from different levels of gas phase calculations together with polarizable continuum model calculations. The reduced Raman isotropic frequencies and their corresponding Raman activities for the three diborate species and metaboric acid, using HF/6-31G*, HF/6-31+G*, HF/6-311+G*, B3LYP/6-31G*, B3LYP/6-31+G*, B3LYP/6-311+G*, MP2/6-31G*, MP2/6-31+G*, and MP2/6-311+G* with a polarizable continuum model, are summarized in Table 2. The Raman activities (intensities) correspond to the unpolarised spectra. Only those expected to give significant intensity in the isotropic spectra (depolarization ratio significantly less than 0.75) are listed. In the discussions below, computational frequencies for comparison with experiment were taken from the MP2/6-311+G* results in Table 2.

The $[B_2O(OH)_5]^-$ species is calculated to have two bands, one in the range 700–750 cm^{-1} and the other in the range 910–975 cm^{-1}, depending upon the level of theory and basis set (Table 2). The $[B_2(OH)_7]^-$ species also was also calculated to have two strong bands, with a peak in the range 690–740 cm^{-1} and another in the range 830–890 cm^{-1}. The divalent species $[B_2O_2(OH)_4]^{2-}$ is predicted to have a very strong band in the region 830 to 850 cm^{-1}, which may correspond to the experimental band at 865 cm^{-1}, but the absence of a weak band near 600 cm^{-1} appears to rule it out. The other divalent species, $[B_2O(OH)_6]^{2-}$, was found to have only one strong calculated band centered in the region 700–740 cm^{-1}, and therefore cannot be the source of the experimental band at 865 cm^{-1}. Although the computational results for mononuclear metaborate $[BO(OH)_2]^-$ do yield a very strong band at 888 cm^{-1}, the very strong bands predicted to be at ~1050 cm^{-1} and 1450 cm^{-1} are completely absent in the experimental spectra.

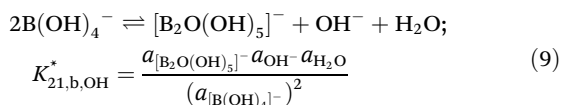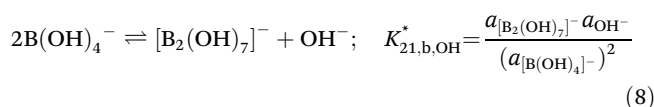## 5. Chemical equilibrium modelling

5.1. Modelling considerations

5.1.1. Choice of potential diborate species for further modelling. The Raman spectra predictions from the MP2/6-311+G* computational results presented above, yielded four ionic species with very strong bands in the range of interest, (865 ± 80) cm^{-1}. The diborates $[B_2(OH)_7]^-$ and $[B_2O(OH)_5]^-$ were predicted to have bands at 848 cm^{-1} and 925 cm^{-1}, respectively. In addition, they are predicted to have strong bands at 719 cm^{-1} and 728 cm^{-1}, respectively, which may underlie the
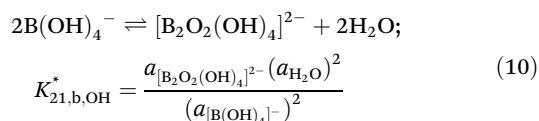
borate band at 745 cm^{-1}. The divalent species $[B_2O_2(OH)_4]^{2-}$ was considered less likely to be the major species contributing to the experimental band at 865 cm^{-1}, because of the absence of a weak band near 600 cm^{-1} and charge balance considerations described below. Although the metaborate ion $[BO(OH)_2]^-$ shows a very strong computational band at 835 cm^{-1}, it was ruled out by the absence of strong and very strong bands at 1049 cm^{-1} and 1451 cm^{-1} in the experimental spectra.

The classic potentiometric study by Mesmer et al.[14] identified a singly-charged diborate ion as a statistically significant species from 50 to 200 °C. As a result, it seems likely that the new species is one or both of the diborates $[B_2(OH)_7]^-$ and $[B_2O(OH)_5]^-$, with $[B_2O_2(OH)_4]^{2-}$ possibly also present as an equilibrium species at temperatures above 200 °C. Thus, the relevant diborate reactions to be considered in developing a chemical equilibrium model are:

$$2B(OH)_4^- \rightleftharpoons [B_2(OH)_7]^- + OH^-; \quad K_{21,b,OH}^* = \frac{a_{[B_2(OH)_7]^-} \, a_{OH^-}}{\left(a_{[B(OH)_4]^-}\right)^2}$$

$$(8)$$

$$2B(OH)_4^- \rightleftharpoons [B_2O(OH)_5]^- + OH^- + H_2O;$$
$$K_{21,b,OH}^* = \frac{a_{[B_2O(OH)_5]^-} \, a_{OH^-} \, a_{H_2O}}{\left(a_{[B(OH)_4]^-}\right)^2}$$

$$(9)$$

and, possibly,

$$2B(OH)_4^- \rightleftharpoons [B_2O_2(OH)_4]^{2-} + 2H_2O;$$
$$K_{21,b,OH}^* = \frac{a_{[B_2O_2(OH)_4]^{2-}} \, (a_{H_2O})^2}{\left(a_{[B(OH)_4]^-}\right)^2}$$

$$(10)$$

Here, the asterisk notation, $Q_{21,b,OH}^*$, indicates cumulative formation of the diborate from $B(OH)_4^-$ rather than $B(OH)_3$. Eqn (8) to (10) are expressed as formation reactions from borate rather than boric acid because the equilibrium molalities of $B(OH)_3$ are negligible at the hydroxide concentrations used in Solutions 4 and 5.

The modelling approach adopted here was based on boron mass balance. Speciation calculations were carried out using the experimental peak areas of the three bands, the boron mass balance, and the known scattering coefficients of $B(OH)_3$ and $[B(OH)_4]^-$,[8,9] from the expression:

$$m_i = \left(\frac{S_{IS}}{S_i}\right) \cdot \left(\frac{A_i}{A_{IS}}\right) \cdot m_{IS}$$

$$(11)$$

Here, m_i and m_{IS} are the molalities of the species i and the perchlorate internal standard, IS, respectively; S_i/S_{IS} is the relative scattering coefficient for species i with respect to the internal standard; A_i and A_{IS} are the peak areas of species i, and the internal standard, respectively. The values for the relative scattering coefficients S_i/S_{IS} for $B(OH)_3$ and $[B(OH)_4]^-$ were taken from Applegarth et al.[9] and Sasidharanpillai et al.[8] Although both monovalent species $[B_2(OH)_7]^-$ and $[B_2O(OH)_5]^-$ are predicted to have two strong bands in the frequency range relevant to this study, $[B_2(OH)_7]^-$ was selected because Gaussian

calculations typically under-predict, rather than over-predict the experimental vibrational frequency.[23] The divalent species with $[B_2O_2(OH)_4]^{2-}$ was also included in the chemical equilibrium modelling as a less likely candidate species.

5.1.2. Identifying the "best" diborate chemical model. To carry out the speciation analysis, the reduced isotropic spectrum of the diborate species was assumed to consist of the strong band at 865 cm^{-1}, and a second band underlying the borate peak at 745 cm^{-1}, with relative intensities (relative scattering coefficients) of $S_{B_2,745}/S_{B_2,865}$, where $S_{B_2,745}/S_{B_2,865}$ is defined as the scattering coefficient ratio of diborate peaks at 745 cm^{-1} and 865 cm^{-1}. Trial values of $S_{B_2,745}/S_{B_2,865}$ were then used to estimate the contribution of $[B_2(OH)_7]^-$ to the total area of the peak at 745 cm^{-1} using eqn (12), and to the peak area of borate using eqn (13):

$$A_{B_2,745} = \frac{S_{B_2,745}}{S_{B_2,865}} \cdot A_{B_2,865}$$

$$(12)$$

$$A_{Borate,745} = A_{total,745} - A_{B_2,745}$$

$$(13)$$

where $A_{B_2,745}$, $A_{Borate,745}$ and $A_{total,745}$ are the areas corresponding to diborate at 745 cm^{-1}, borate at 745 cm^{-1} and total area of the peak at 745 cm^{-1}, respectively. Three choices for the scattering coefficient of the diborate band at 745 cm^{-1}, relative to the band at 865 cm^{-1} were considered: $S_{B_2,745}/S_{B_2,865}$ = 0 (Model 1); $S_{B_2,745}/S_{B_2,865}$ = 0.95 (Model 2); and $S_{B_2,745}/S_{B_2,865}$ = 1.5 (Model 3). Model 1 is applicable to diborate species postulated to have no band at 745 cm^{-1}, corresponding exclusively to band "X" in Fig. 2. Models 2 and 3 were based on the MP2/6-311+G* computational values of $S_{B_2,745}/S_{B_2,865}$ for $[B_2(OH)_7]^-$ and $[B_2O(OH)_5]^-$, respectively, in Table 2. Although computational Raman scattering intensities are known to be quite unreliable,[21,25] the calculated relative Raman intensities of two bands within the same molecule are expected to be more accurate.

Models 1 and 3 proved to be not consistent with the physico–chemical constraints. For Model 1, the experimental scattering coefficient of the 865 cm^{-1} band relative to that of the perchlorate internal standard $S_{B_2,865}/S_{IS}$ was found to increase by about 300% from 150 °C to 300 °C, and had significant discrepancies in the charge balance of Solutions 1 and 2 of +10% at 150 °C, rising to +20% at 300 °C. Model 3 had an almost constant scattering coefficient, but a negligible concentration of $[B(OH)_4]^-$ at 300 °C, which contradicts the results of previous studies by Mesmer et al.,[14] Wang et al.[17] and Palmer et al.[26]

Model 2 yielded scattering coefficients that were independent of concentration and temperature above 150 °C, $S_{B_2,865}/S_{IS}$ = 0.107 ± 0.015. The charge balances had small systematic discrepancies. For Solutions 1 and 2 it was too positive (~15% at 150 °C rising to ~30% above 200 °C), and for Solutions 5 and 6 at 250 °C it was similarly elevated (~+12% after the effect of the excess NaCl and LiCl was subtracted) (ESI, Table S2†). Varying the relative scattering coefficient of the diborate bands by ±10% did not significantly change the internal consistency of the treatment. Representative fits for
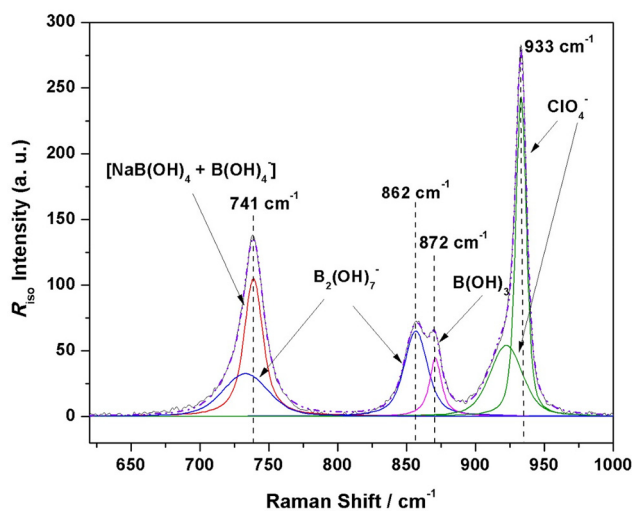
Fig. 6 Reduced isotropic Raman spectra of NaB(OH)$_4$(aq.), $R_{Iso}(\bar{\nu})$, at 250 °C and 20 MPa from Fig. 2, indicating the calculated hypothetical contributions to the 745 cm^{-1} band from [B(OH)$_4$]$^-$ and [B$_2$(OH)$_7$]$^-$ corresponding to a relative scattering factor for the diborate ion bands of $S_{B_2,745}/S_{B_2,865} = 0.95$, as predicted by the DFT calculations.

the reduced isotropic Raman spectra using Model 2 for Na (BOH)$_4$(aq.), $R_{Iso}(\bar{\nu})$, at 250 °C and 20 MPa are shown in Fig. 6. The calculated equilibrium molalities and diborate scattering coefficients using Model 2 are tabulated in Table 3.

These results provide strong evidence for the presence of a new species that is a diborate ion, with bands in the 745 region and at 865 cm^{-1}, $S_{B_2,745}/S_{B_2,865} = 0.95 \pm 0.10$. The analysis above suggests that the new species is very probably [B$_2$(OH)$_7$]$^-$. A factor analysis of the Raman spectra at 250 °C was performed, using the singular value decomposition 'svds' function on Matlab R2021b. Although the data set was limited and mathematically underdetermined, there were four statistically significant factors. In addition to the peaks at 739.4 cm^{-1} (borate) and 874.0 cm^{-1} (boric acid), there were also major peaks identified at 737.5 cm^{-1} and 863.7 cm^{-1}, and minor peaks at 746.9 cm^{-1}, 754.5 cm^{-1}, 853.3 cm^{-1}, and 866.0 cm^{-1}, at 250 °C, supporting the model with a new species having a Raman peak around ~750 and 865 cm^{-1}.

The charge-balance discrepancy and the factor analysis of the high temperature Raman data, suggest that another anionic boron species may be present as a minor equilibrium species, possibly [B$_2$O$_2$(OH)$_4$]$^{2-}$. Adding a contribution from the minor divalent species to the band at 865 cm^{-1} did not lead to an improved model. The possibility that [B$_2$O(OH)$_6$]$^{2-}$ might have been present was addressed by adding a divalent anionic species to the 745 cm^{-1} band in the models noted above and varying the relative scattering coefficients of both diborate species. However, it was not possible to achieve fully temperature-independent scattering coefficients and charge balance.

Additional evidence that the 865 cm^{-1} band is not due to [B$_2$O(OH)$_6$]$^{2-}$ or [BO(OH)$_2$]$^-$ is provided by the effect of hydroxide on the reduced isotropic Raman spectra at 250 °C. As can

be seen in Reactions 8 and 9, hydroxide participates directly in the formation of these two diborate ions from borate. However, the divalent diborate species [B$_2$O(OH)$_6$]$^{2-}$ and metaborate form by condensation reactions which are not pH dependent, as described in Reaction 14 and by:

$$[B(OH)_4]^- \rightleftharpoons [BO(OH)_2]^- + H_2O \qquad (14)$$
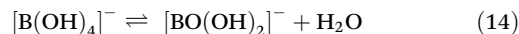
It is clear from the stoichiometry of these reactions that the equilibria to form monovalent [B$_2$(OH)$_7$]$^-$ and/or its condensed product [B$_2$O(OH)$_5$]$^-$ are affected by changes in the concentration of OH$^-$, whereas the formation of [B$_2$O(OH)$_6$]$^{2-}$ and/or [BO(OH)$_2$]$^-$ are not. The constant values for the relative scattering factors in Table 3, calculated from the relative peak areas of the 745 cm^{-1} and 865 cm^{-1} bands for Solutions 3 and 4 using Model 2, support the conclusion that [B$_2$(OH)$_7$]$^-$ and/or [B$_2$O(OH)$_5$]$^-$ are the equilibrium diborate species. This is consistent with the potentiometric studies reported by Mesmer et al.[14] who identified the presence of a singly charged diborate species in sodium borate solutions at higher temperature, and postulated the existence of the [B$_2$(OH)$_7$]$^-$ species. The consistent value obtained for the scattering factors at other temperatures over the range 200 to 300 °C, $S^r_{[B_2(OH)_7]^-} \approx 0.107 \pm 0.015$, despite changes in pH associated with changes in the boric acid ionization constant further supports this conclusion.

Based on the evidence presented above, our analysis was based on the premise that [B$_2$(OH)$_7$]$^-$ is the major equilibrium diborate species, and that polyborate formation quotients could be determined using the concentrations from Model 2.

5.2. Equilibrium chemical speciation and diborate formation quotients

The equilibrium quotient for [B$_2$(OH)$_7$]$^-$ diborate formation from the borate ion, according to reaction (8), was calculated from the expression:

$$Q^\star_{21,b,OH} = \frac{m_{[B_2(OH)_7]^-} \cdot m_{OH^-}}{(m_{B(OH)_4^-})^2} \qquad (15)$$

using the experimental molalities of the species calculated from Model 2. Here, the asterisk notation, $Q^\star_{21,b,OH}$, indicates cumulative formation of the diborate from B(OH)$_4^-$ rather than B(OH)$_3$.

The experimental molalities of each species and resulting formation quotients for B$_2$(OH)$_7^-$ are tabulated in Table 3. For Solutions 3 and 4, the molalities of the hydroxide ions required for these calculations were calculated from charge and mass balance. For all other solutions, which had buffer ratios $R_{Buffer} \approx 1$, the hydroxide molalities were derived from the experimental borate and boric acid molalities, and the expression for the ionization constant of boric acid reported by Palmer et al.,[26] as described in our previous study.[8]

The diborate formation quotients from Table 3 for Solutions 1 and 2 (NaBOH$_4$(aq.), $R_{Buffer} = 1$, $m = 1$ mol kg^{-1}) are plotted as a function of temperature in Fig. 7, where they are compared to the equilibrium constants reported by

Table 3 Experimental solvent densities, equilibrium molalities for boron species and hydroxide, the relative scattering coefficient, $S^r_{B_2,865} = (S_{[B_2(OH)_7]^-}/S_{ClO_4^-})$ and the resulting formation constants $Q^*_{21,b,OH}$ for diborate at $p = 20$ MPa. The relative scattering coefficients for the diborate bands 745 and 865 cm⁻¹ where taken to be $S_{B_2,745}/S_{B_2,865} = 0.95 \pm 0.10$ (Model 2)[a]

$t/°C$	ρ_w/kg m⁻³	$m_{B(OH)_3}$	$m_{[B(OH)_4]^-}$	$m_{[B_2(OH)_7]^-}$	$m_{(OH)^-}$	$S^r_{[B_2(OH)_7]^-}$	I/mol kg⁻¹	$\log Q^*_{21,b,OH}$ Exp.	$\log Q^*_{21,b,OH}$ Wang et al.[17]	$\log K^*_{21,b,OH}$ Palmer[24]
				× 10³/mol kg⁻¹						
				Solution 1 (Run 1), $R_{Buffer} = 0.980$, $m_B = 1.0188$ mol kg⁻¹						
150	927.69	18.6 ± 1.4	616 ± 43	192 ± 21	47.65	(0.060 ± 0.008)	1.017	−1.618	−3.233	−2.512
200	877.97	44.0 ± 3.7	534 ± 53	220 ± 26	49.56	0.092 ± 0.013	0.991	−1.416	−3.002	−2.107
250	816.09	69.1 ± 4.0	339 ± 24	305 ± 12	41.04	0.106 ± 0.006	0.932	−0.962	−2.880	−1.878
275	778.71	73.4 ± 4.1	220 ± 29	363 ± 15	32.50	0.112 ± 0.007	0.897	−0.615	−2.860	−1.791
300	734.71	85.9 ± 3.2	275 ± 20	329 ± 10	42.25	0.129 ± 0.006	0.912	−0.736	−2.866	−1.691
				Solution 1 (Run 2), $R_{Buffer} = 0.980$, $m_B = 1.0188$ mol kg⁻¹						
150	927.69	22.1 ± 1.9	619 ± 47	189 ± 23	40.33	(0.070 ± 0.010)	1.013	−1.700	−3.233	−2.512
200	877.97	33.2 ± 3.3	490 ± 49	248 ± 24	60.27	0.092 ± 0.011	0.988	−1.206	−3.002	−2.107
250	816.09	64.3 ± 6.7	326 ± 61	314 ± 31	42.47	0.109 ± 0.016	0.930	−0.900	−2.880	−1.878
				Solution 2, $R_{Buffer} = 0.984$, $m_B = 1.0391$ mol kg⁻¹						
150	927.69	18.5 ± 3.5	648 ± 28	186 ± 14	50.20	(0.067 ± 0.007)	1.049	−1.652	−3.243	−2.512
200	877.97	42.4 ± 2.8	482 ± 32	257 ± 16	46.32	0.084 ± 0.007	1.000	−1.290	−3.014	−2.107
250	816.09	66.9 ± 4.8	315 ± 38	329 ± 19	39.40	0.099 ± 0.009	0.949	−0.883	−2.891	−1.878
				Solution 3, $R_{Buffer} = 1.716$, $m_B = 0.96404$ mol kg⁻¹						
150	927.69	0.95 ± 0.15	629 ± 25	167 ± 13	857.6	(0.109 ± 0.009)	1.832	−0.440	−3.426	−2.512
200	877.97	2.23 ± 0.64	513 ± 55	225 ± 27	915.8	0.109 ± 0.016	1.862	−0.104	−3.237	−2.107
250	816.09	3.20 ± 0.68	350 ± 41	305 ± 20	996.9	0.126 ± 0.012	1.902	0.397	−3.111	−1.878
				Solution 4, $R_{Buffer} = 3.542$, $m_B = 0.90062$ mol kg⁻¹						
150	927.69	0.35 ± 0.09	668 ± 30	116 ± 15	2406	(0.100 ± 0.015)	3.336	−0.377	−3.767	−2.512
200	877.97	0.95 ± 0.14	450 ± 27	225 ± 14	2515	0.097 ± 0.007	3.391	0.461	−3.606	−2.107
250	816.09	2.64 ± 0.39	368 ± 27	265 ± 14	2555	0.101 ± 0.008	3.411	0.964	−3.431	−1.878
				Solution 5a, $R_{Buffer} = 0.980$, $m_B = 0.32012$ mol kg⁻¹						
250	816.09	36.5 ± 2.0	78.1 ± 9.7	103 ± 5.0	19.51	120 ± 0.009	0.285	−0.483	−2.152	−1.878
				Solution 5b, $R_{Buffer} = 0.980$, $m_B = 0.32012$ mol kg⁻¹ + 0.301 mol kg⁻¹ NaCl						
250	816.09	32.1 ± 2.5	82.0 ± 13.7	103 ± 7.0	21.97	0.127 ± 0.013	0.590	−0.472	−2.681	−1.878
				Solution 6a,[b] $R_{Buffer} = 0.980$, $m_B = 0.30980$ mol kg⁻¹						
250	816.09	34.1 ± 2.0	56.8 ± 7.9	109 ± 4.1	15.22	0.090 ± 0.007	0.279	−0.287	−2.520	−1.878
				Solution 6b,[b] $R_{Buffer} = 0.980$, $m_B = 0.30980$ mol kg⁻¹ + 0.302 mol kg⁻¹ LiCl						
250	816.09	40.1 ± 2.8	66.0 ± 11.3	102 ± 5.8	14.18	0.124 ± 0.012	0.581	−0.479	−3.024	−1.878

[a] Uncertainties are propagated standard errors from the fitted Voight functions. Values in parentheses have scattering coefficients beyond the 90% confidence limit of the mean, $S^r_{B_2,865} = 0.107 \pm 0.015$, and were considered to have systematic errors. $\log Q^*_{21,b,OH}$, from Wang et al.[17] were calculated for similar R_{buffer} using OLI Studio but for the formation of $B_2O(OH)_5^-$. $\log K^*_{21,b,OH}$, from Palmer were calculated from $\log K_{11}$ and $\log K_{12}$ expressions in Ref. 24. [b] $LiB(OH)_4$ solution.

Ferguson et al.[27] and Palmer et al.[26] Van't Hoff fits to the experimental formation quotients at ionic strength $I = 1$ mol kg⁻¹ from this work (Solutions 1 and 2) and from Mesmer et al.[14] yield the expressions:

$$\log Q^*_{21,b,OH}(T, I = 1 \text{ mol kg}^{-1})$$
$$= (-1673 \pm 171) + (2.28 \pm 0.35)/T \quad (16)$$

and

$$\log Q^*_{21,b,OH}(T, I = 1 \text{ mol kg}^{-1})$$
$$= (-2182 \pm 153) + (2.42 \pm 0.35)/T \quad (17)$$

respectively. The experimental values of $\log Q^*_{21,b,OH}$ from this study are systematically higher than Mesmer's potentiometric

values at the same ionic strength. The difference decreases with increasing temperature.

The formation quotients from this Raman study are in very good agreement with those from the conductivity measurements by Ferguson et al.,[27] despite the fact that these are very different methods with different assumptions and approximations. We note that these Raman and conductivity measurements were all carried out on $NaB(OH)_4$ solutions at molalities from 0.2 mol kg⁻¹ to 1 mol kg⁻¹, with or without excess NaOH, in which diborate is a major species. The potentiometric measurements by Mesmer et al. were carried in 1 mol kg⁻¹ KCl solutions with boron concentrations from 0.03 to 0.5 mol kg⁻¹, at equilibrium hydroxide concentrations below 0.01 mol kg⁻¹, in which diborate was a minor species. This raises the possi-
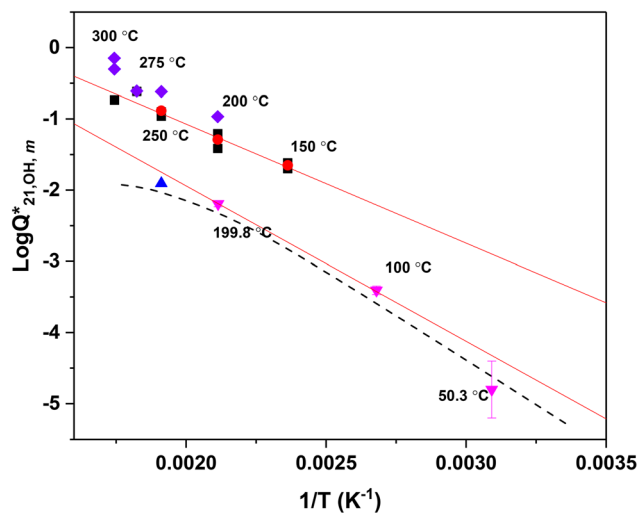
Fig. 7 Plot of log $Q^*_{21,b,OH}$ as a function of temperature $(1/T)$ at $p = 20$ MPa from this work and at p_{sat} from Mesmer's experimental data.[14] The filled black squares (■) and filled red circles (●) represent the experimental log $Q^*_{21,b,OH}$ for Solutions 1 and 2, respectively. The pink triangles (▼) are Mesmer's experimental data[14] at 50, 100, and 200 °C. The blue triangle (▲) is the extrapolated value at 250 °C from Mesmer's data by Palmer *et al.*[26] The red lines are the van't Hoff fits to the experimental data from this work and from Mesmer *et al.* at $I = 1$ mol kg^{-1}, eqn (16) and (17). The purple diamonds (◆) represent the formation constants from conductivity experiments.[26]
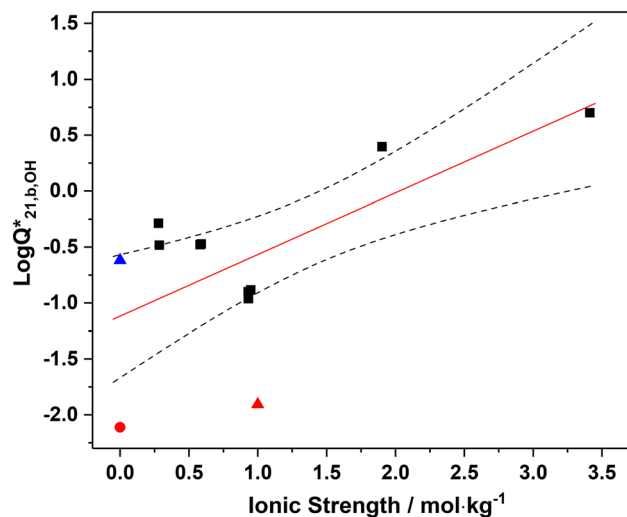

Fig. 8 Plot of log $Q^*_{21,b,OH}$ as a function of ionic strength at 250 °C at $p = 20$ MPa. The black squares (■) are the experimental values from this work. The blue triangle (▲) represents the value from conductivity experiments by Ferguson *et al.*[27] The red triangle (▲) and circle (●) are Mesmer's value of log $Q^*_{21,b,OH}$ at $I = 1$ mol kg^{-1} and $I = 0$, extrapolated to 250 °C by Palmer *et al.*[26] The red line is the weighted linear fit to the Raman data, given by eqn (20), The 90% confidence limits for the linear model are shown by the dashed black curves.

bility that a second species, possibly a sodium ion pair, is contributing to the formation constants reported as $Q^*_{21,b,OH}$ in Table 3 and Fig. 7.

5.3. Diborate formation constants

The equilibrium constant for diborate formation, $K^*_{21,b,OH}$, is given by the expression:

$$K^*_{21,b,OH} = Q^*_{21,b,OH} \times Q^*_{\gamma,21,b,OH} \tag{18}$$

where the terms

$$Q^*_{21,b,OH} = \frac{m_{[B_2(OH)_7]^-} \cdot m_{OH^-}}{\left(m_{B(OH)_4^-}\right)^2} \text{ and } Q^*_{\gamma,21,b,OH} = \frac{\gamma_{[B_2(OH)_7]^-} \cdot \gamma_{OH^-}}{\left(\gamma_{B(OH)_4^-}\right)^2} \tag{19}$$

are the formation quotient and activity coefficient quotient, respectively. The composition-dependence of the experimental formation quotients at 250 °C is plotted as a function of the ionic strength in Fig. 8, along with extrapolated values from Mesmer and Palmer *et al.*,[26] and the experimental value from Ferguson *et al.*[27] The plot also shows the results of fitting these values with linear regression, using weighting factors proportional to the total boron concentration of each solution, to yield the expression:

$$\log Q^*_{\gamma,21,b,OH} = \log K^*_{21,b,OH} - aI \tag{20}$$

Where log $K^*_{21,b,OH} = -1.20 \pm 0.229$ and $a = 0.639 \pm 0.134$. The uncertainties are standard errors.

For consistency with our previous Raman study on the formation constants of triborate,[8] an attempt was made to model the activity coefficient quotient using the same treatment, which is based on the expressions developed by Palmer *et al.*[26] A simple treatment was also used in which the activity coefficients were assumed to depend only on ionic charge, so that:

$$\gamma_{[B_2(OH)_7]^-} = \gamma_{[B(OH)_4]^-} = \gamma_{OH^-} \tag{21}$$

and

$$K^*_{\gamma,21,b,OH} = Q^*_{\gamma,21,b,OH}. \tag{22}$$

Neither model predicted the steep ionic-strength dependence of log $Q^*_{21,b,OH}$ shown in Fig. 8.

6. Discussion

6.1. Composition dependence of $Q^*_{21,b,OH}$ and evidence for a second diborate species

As noted in section 5.2, the formation quotients from this Raman study are in very good agreement with those from the conductivity measurements by Ferguson *et al.*,[27] yet are systematically larger than the potentiometric results reported by Mesmer *et al.*, which were measured in KCl solutions at lower pH. The composition-dependent equilibrium constants plotted in Fig. 8 are consistent with these trends and since the magnitude of log K increases with the molalities of Na$^+$ and OH$^-$. Noting that the effect of hydroxide on the equilibrium

between $[B_2(OH)_7]^-$ and $[B_2O_2(OH)_4]^{2-}$ is governed by a reaction that directly involves hydroxide,

$$[B_2(OH)_7]^- + OH^- \rightleftharpoons [B_2O_2(OH)_4{}^{2-}] + 2H_2O \qquad (23a)$$
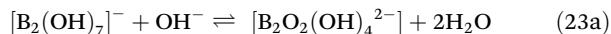
we speculate that this may be evidence for the presence of $[B_2O_2(OH)_4]^{2-}$, in the form of a contact ion pair.

$$[B_2(OH)_7]^- + OH^- + Na^+ \rightleftharpoons Na[B_2O_2(OH)_4]^- + 2H_2O \qquad (23b)$$
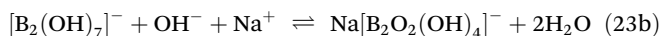
The band assignments used to derive the formation quotients reported in Table 3 are based on the computationally predicted vibrational frequencies listed in Table 2 and the assumption that no polyborate species other than $[B_2(OH)_7]^-$ and/or $[B_2O(OH)_5]^-$ contributes to the intensity of the 865 cm^{-1} band. While the computational spectrum of $[B_2O_2(OH)_4]^{2-}$ also showed an intense band near 865 cm^{-1}, it was rejected on the grounds that no weak band near 600 cm^{-1} was observed in the experimental spectra. This objection may not be valid in the case of the $[B_2O_2(OH)_4]^{2-}$ contact ion pair. With reference to the structure in Fig. 5, the predicted band near 865 cm^{-1} is essentially the symmetric B–O(H) stretch, while the band near 600 cm^{-1} primarily due to the in-plane B_2O_2 deformation, with some coupling to the BOH bending mode. The formation of a contact ion-pair with Na$^+$ at the ring site would be expected to shift the 600 cm^{-1} band to higher frequencies and to reduce its intensity.

6.2. Uncertainties in the diborate formation quotients

The formation quotients for $[B_2(OH)_7]^-$ from this work, plotted in Fig. 7 and 8, show a much larger experimental scatter than has been observed in similar studies using the same methods.[8,9] The uncertainties arise, in part, from the possible contribution of $Na[B_2O_2(OH)_4]^-$ to the 865 cm^{-1} band, and in the need to resolve the relative contributions of the diborate species and $[B(OH)_4]^-$ to the band at 745 cm^{-1}. The interpretation is complicated further by the inability of Raman spectroscopy to distinguish between the free borate ion, $[B(OH)_4]^-$ and the sodium borate ion-pair, $[NaB(OH)_4]^0$.[9,12] Calculations based on the ion-pair formation constants reported by Arcis *et al.*[28] suggest that the majority of the aqueous borate species at these concentrations may in fact be solvent-separated ion pairs. As a result, the bands at 745 and 865 cm^{-1} may also include contributions from sodium ion pairs with diborate, $[NaB_2(OH)_7]^0$, which presents a similar hydroxyl-rich surface to the surrounding hydration shell. Accurate measurements over a much wider range of solution compositions and the full temperature range would be needed to resolve these issues.

6.3. Impact on chemical speciation models for aqueous boron

The complex aqueous speciation chemistry of boron is of critical interest to the nuclear industry, and is relevant to a number of other sectors including geology/geochemistry, natural waters, and various chemical and industrial processes. In the nuclear industry, two major software packages are used for modeling chemical speciation in reactor coolant. These are

based on different chemical equilibrium models and independent critically evaluated thermodynamic data.[26,29] The Electric Power Research Institute's (EPRI) chemical modelling software, MULTEQ, which is distributed as part of ChemWorks Tools (v.7.0), makes use of a "model species" activity coefficient treatment, the Meissner equation,[30] and is most accurate at ionic strengths below 1 mol kg^{-1}. The OLI Analyzer Studio 9.2.1 software (OLI Systems Inc.), is based on standard-state properties from the Helgeson–Kirkham–Flowers (HKF) equation[31,32] and the mixed-solvent electrolyte (MSE) model for excess properties from Anderko *et al.*[33] MULTEQ and OLI have adopted different chemical formulations for the diborate ion. MULTEQ defines the diborate ion as $[B_2(OH)_7]^-$, while OLI Studio defines diborate as the condensed species $[B_2O(OH)_5]^-$. It is also important to note that MULTEQ uses the equation reported by Marshall and Franck[34] for the ionization constant of water, K_w, while OLI uses the expression derived for the HKF model.[31,32] The critically-evaluated values for speciation, phase equilibria, and other thermodynamic properties of boron-containing systems in the OLI Analyzer Studio 9.2.1 have been reported by Wang *et al.*[17]

A revision to the databases of both MULTEQ and OLI Studio to include the new diborate formation quotients from this study, should include the results from our earlier work on the formation constants for the triborate ion.[8] The spectra reported for the more acidic boric acid/borate solutions in the triborate study, impose an upper limit on the formation constant of $[B_2(OH)_7]^-$ because the presence of diborate as an equilibrium species at concentrations above the detection limit of 0.1 mol kg^{-1} would have been observable as a weak band at 865 cm^{-1} when, in fact, no such bands were seen. This upper limit is more consistent with the formation constant reported by Palmer, than with the results in Table 3 and Fig. 7, consistent with presence of a second diborate species as discussed above.

The implication of these results for model database development are twofold. First, the experimental results demonstrate that the $[B_2(OH)_7]^-$ ion is a significant species that may form under 'hideout'-type conditions in nuclear power reactors, and in hydroxide-rich borate solutions at elevated temperatures in other chemical and industrial processes. Second, the divalent ion $[B_2O_2(OH)_4]^{2-}$ may also be present as an ion pair with alkali metal ions and may also affect boron hideout chemistry. Finally, as noted above, the Raman spectra of borate solutions in our recent triborate publication show that these diborate species are not expected to present at high enough concentrations to significantly affect the bulk primary coolant chemistry in PWR nuclear reactors.

7. Conclusions

The presence of a previously unreported equilibrium aqueous boron species has been identified by Raman spectroscopy in ~1 mol kg^{-1} NaB(OH)$_4$ solutions at temperatures from 150 to 300 °C and 20 MPa. The most plausible polyborate species

structures were examined computationally, as well as by observing the effects of excess Li^+, Na^+, and OH^- ions on the experimental Raman spectra. The experimental results, together with the computational frequency predictions, indicate that the most likely candidate for the boron species are $[B_2(OH)_7]^-$ and/or $[B_2O(OH)_5]^-$, which is consistent with Mesmer's potentiometric studies.[14] The DFT-predicted frequencies suggest that $[B_2(OH)_7]^-$ is the more likely candidate for the major species. The Raman scattering coefficients, equilibrium concentrations, and formation constants were calculated from three different modelling approaches based on peak area and mass balance. The models had charge-balance discrepancies for solutions in which hydroxide concentrations were calculated using the boric acid ionization constants and activity coefficient model reported by Palmer *et al.*,[26] however, Model 2 yielded constant scattering coefficients within the experimental uncertainties, while other models did not. As a result of this finding and of the DFT-predicted vibrational spectra, the formation quotients for $[B_2(OH)_7]^-$, $Q^*_{21,b,OH}$, calculated from the equilibrium concentrations determined using Model 2 are most consistent with the computational and Raman results.

The formation quotients for $[B_2(OH)_7]^-$, $Q^*_{21,b,OH}$ from both models showed inconsistencies that varied with temperature and composition. These may be due to the presence of another equilibrium species at temperatures above ~150 °C, and/or a strong activity coefficient effect that is not well represented by the models used in this study. If present, the most likely candidate for a second unknown species is the divalent diborate ion pair, $Na[B_2O_2(OH)_4]^-$. The detection limits observed for the Raman spectra of boric-acid rich solutions at these temperatures[8,9] place an upper limit on the standard-state formation constants of $[B_2(OH)_7]^-$ at all the temperatures studied.

Author contributions

Swaroop Sasidharanpillai: data curation, formal analysis, investigation, methodology, validation, writing – original draft, writing – review & editing. Jenny S. Cox: data curation, investigation, methodology, formal analysis, validation, writing – original draft, writing – review & editing. Cory C. Pye: investigation, formal analysis, methodology, writing – original draft. Peter R. Tremaine: conceptualization, formal analysis, methodology, project administration, supervision, validation, visualization, funding acquisition, writing – original draft, writing – review & editing, resources.

Conflicts of interest

There are no conflicts of interest to declare.

Acknowledgements

References

1 L. M. Rowe, L. B. Tran and G. Atkinson, The effect of pressure on the dissociation of boric acid and sodium borate ion pairs at 25 °C, *J. Solution Chem.*, 1989, **18**(7), 675–689.

2 J. Yongzhong, G. Shiyang, X. Shuping and L. Jun, FT-IR, spectroscopy of supersaturated aqueous solutions of magnesium borate, *Spectrochim. Acta, Part A*, 2000, **56**(7), 1291–1297.

3 L. Jun, X. Shuping and G. Shiyang, FT-IR and, Raman spectroscopic study of hydrated borates, *Spectrochim. Acta, Part A*, 1995, **51**(4), 519–532.

4 R. E. Weston, Raman Spectra of Electrolyte Solutions in Light and Heavy Water, *Spectrochim. Acta*, 1962, **18**(9), 1257–1277.

5 C. Schmidt, R. Thomas and W. Heinrich, Boron speciation in aqueous fluids at 22 to 600 °C and 0.1 MPa to 2 GPa, *Geochim. Cosmochim. Acta*, 2005, **69**(2), 275–281.

6 Y. Q. Zhou, C. H. Fang, Y. Fang and F. Y. Zhu, Polyborates in aqueous borate solution: A Raman and DFT theory investigation, *Spectrochim. Acta, Part A*, 2011, **83**(1), 82–87.

7 F. Y. Zhu, C. H. Fang, Y. Fang, Y. Q. Zhou, H. W. Ge and H. Y. Liu, Structure of aqueous potassium pentaborate solution, *J. Mol. Struct.*, 2015, **1083**, 471–479.

8 S. Sasidharanpillai, H. Arcis, L. Trevani and P. R. Tremaine, Triborate Formation Constants and Polyborate Speciation under Hydrothermal Conditions by Raman Spectroscopy using a Titanium/Sapphire Flow Cell, *J. Phys. Chem. B*, 2019, **123**(24), 5147–5159.

9 L. M. S. G. A. Applegarth, C. C. Pye, J. S. Cox and P. R. Tremaine, Raman Spectroscopic and ab Initio

Investigation of Aqueous Boric Acid, Borate, and Polyborate Speciation from 25 to 80 °C, *Ind. Eng. Chem. Res.*, 2017, **56**(47), 13983–13996.

10 F. Y. Zhu, C. H. Fang, Y. Fang, Y. Q. Zhou, H. W. Ge and H. Y. Liu, Structure of aqueous potassium metaborate solution, *J. Mol. Struct.*, 2014, **1070**, 80–85.

11 C. H. Fang, F. Y. Zhu, Y. Fang, Y. Q. Zhou, S. Tao and S. Xu, Structure of aqueous potassium tetraborate solutions by X-ray scattering, *Phys. Chem. Liq.*, 2013, **51**(2), 218–232.

12 R. Buchner, G. Hefter, P. M. May and P. Sipos, Dielectric relaxation of dilute aqueous NaOH, NaAl(OH)₄, and NaB (OH)₄, *J. Phys. Chem. B*, 1999, **103**(50), 11186–11190.

13 K. Ishihara, A. Nagasawa, K. Umemoto, H. Ito and K. Saito, Kinetic Study of Boric Acid-Borate Interchange in Aqueous Solution by 11B NMR Spectroscopy, *Inorg. Chem.*, 1994, **33**(17), 3811–3816.

14 R. E. Mesmer, C. F. Baes and F. H. Sweeton, Acidity measurements at elevated temperatures. VI. Boric acid equilibriums, *Inorg. Chem.*, 1972, **11**(3), 537–543.

15 C. F. Baes and R. E. Mesmer, *The Hydrolysis of Cations*, John Wiley & Sons, New York, 1976.

16 N. Ingri, G. Lagerström, M. Frydman and L. G. Sillén, Equilibrium Studies of Polyanions. II. Polyborates in NaClO₄ Medium, *Acta Chem. Scand.*, 1957, **11**, 1034–1058.

17 P. Wang, J. Kosinski Jerzy, M. Lencka Malgorzata, A. Anderko and D. Springer Ronald, Thermodynamic modeling of boric acid and selected metal borate systems, *Pure Appl. Chem.*, 2013, **85**(11), 2117–2144.

18 W. T. Lindsay, Jr., in Chemistry of Steam Cycle solutions: Principles, in *The ASME Handbook on Water Technology for Thermal Power Systems*, ed. P. Cohen, Amer. Soc. Mech. Eng., New York, 1989, pp. 341–544.

19 W. T. Lindsay Jr, MULTEQ: What it is and what it can do, in *Control of Corrosion on the Secondary side of Steam Generators*, ed. R. W. Staehle, J. A. Gorman and A. R. Mcllree, Nat. Assoc. Corrosion Eng. (NACE), Houston, TX, United States, 1996.

20 M. H. Brooker, O. F. Neilsen and E. Praestgaard, Assessment of Correction Procedures for Reduction of Raman Spectra, *J. Raman Spectrosc.*, 1988, **19**(2), 71–78.

21 C. C. Pye, A Crystallographic Review of Alkali Borate Salts and Ab Initio Study of Borate Ions/Molecules, in *Concepts, Methods and Applications of Quantum Systems in Chemistry and Physics*, ed. Y. A. Wang, M. Thachuk, R. Krems and J. Maruani, Springer International Publishing, Springer, 2018, pp. 107–142.

22 M. H. Brooker and P. R. Tremaine, Raman Studies of Hydration of Hydroxy Complexes and the Effect on Standard Partial Molar Heat Capacities, *Geochim. Cosmochim. Acta*, 1992, **56**(6), 2573–2577.

23 E. Bulemela and P. R. Tremaine, D₂O Isotope Effects on the Ionization of β-Naphthol and Boric Acid at Temperatures from 225 to 300 °C using UV-Visible Spectroscopy, *J. Solution Chem.*, 2009, **38**(7), 805–826.

24 D. A. Palmer, Aqueous Boron Species, in *Chemical Thermodynamics: Ancillary Data. Thermochemical Database Project*, ed. M. Rand, OECD Nuclear Energy Agency, Paris, France, In press.

25 C. C. Pye, An Ab Initio Study of Boric Acid, Borate, and their Interconversion, in *Concepts, Methods and Applications of Quantum Systems in Chemistry and Physics*, ed. Y. A. Wang, M. Thachuk, R. Krems and J. Maruani, Springer International Publishing, Springer Cham, 2018, pp. 143–177.

26 D. A. Palmer, P. Benezeth and D. Wesolowski, Boric acid hydrolysis: A new look at the available data, *Power Plant Chem.*, 2000, **2**(5), 261–264.

27 J. P. Ferguson, *Aqueous Boric Acid Chemistry under Pressurized Water Reactor Coolant Conditions by AC Conductivity*, PhD Thesis, University of Guelph, Guelph, Canada, 2018.

28 H. Arcis, J. P. Ferguson, G. H. Zimmerman and P. R. Tremaine, The limiting conductivity of the borate ion and its ion-pair formation constants with sodium and potassium under hydrothermal conditions, *Phys. Chem. Chem. Phys.*, 2016, **18**(34), 24081–24094.

29 P. Wang, A. Anderko and R. D. Young, A speciation-based model for mixed-solvent electrolyte systems, *Fluid Phase Equilib.*, 2002, **203**(1–2), 141–176.

30 H. P. Meissner and J. W. Tester, Activity Coefficients of Strong Electrolytes in Aqueous Solutions, *Ind. Eng. Chem. Process Des. Dev.*, 1972, **11**(1), 128–133.

31 J. C. Tanger IV and H. C. Helgeson, Calculation of the Thermodynamic and Transport Properties of Aqueous Species at High Pressures and Temperatures: Revised Equations of State for the Standard Partial Molal Properties of Ions and Electrolytes, *Am. J. Sci.*, 1988, **288**, 19–98.

32 E. L. Shock and H. C. Helgeson, Calculation of the thermodynamic and transport properties of aqueous species at high pressures and temperatures: Correlation algorithms for ionic species and equation of state predictions to 5 kb and 1000 °C, *Geochim. Cosmochim. Acta*, 1988, **52**(8), 2009–2036.

33 A. Anderko, P. Wang and M. Rafal, Electrolyte Solutions: From Thermodynamic and Transport Property Models to the Simulation of Industrial Processes, *Fluid Phase Equilib.*, 2002, 123–142.

34 W. L. Marshall and E. U. Franck, Ion Product of Water Substance, 0–1000 °C, 1–10,000 Bars: New International Formulation and Its Background, *J. Phys. Chem. Ref. Data*, 1981, **10**, 295–304.